

MORPHOLOGY, STRUCTURAL AND ELECTRICAL TRANSPORT PROPERTIES OF GRAPHITE BASED MULTILAYER THIN FILMS

A. USMAN^{a*}, M. S. RAFIQUE^b, S.F. SHAUKAT^a, S. ANJUM^c, H. LATIF^d,
A. SATTAR^a

^a*Department of Physics, COMSATS Institute of Information Technology, Lahore, Pakistan*

^b*Department of Physics, University of Engineering & Technology, Lahore, Pakistan.*

^c*Department of Physics, Lahore College for Woman University Lahore, Pakistan.*

^d*Department of Physics, Forman Christian College University Lahore, Pakistan.*

Silver doped graphite multilayer films were grown on silicon substrate by employing a modified pulsed laser ablation (PLA) process. Excimer laser ($\lambda=248\text{nm}$) was used for the deposition of these films. The effects of Ag incorporation on the micro structure as well as on surface morphologies were investigated using Raman Spectroscopy, XRD and AFM. The structural investigation reveals that diamond phase reduces gradually by the incorporation of silver content. It was also observed that Ag doping enhanced the sp^2 fraction in films which is a clear indication of graphitization. The surface analysis revealed that some clustering was observed on the surface which is due to encapsulation of silver nano particles within carbon network. Some elevated textures were also found on surface. A small change in surface roughness was also observed which is ranging from 2.41 nm to 10.1 nm. The optical band gap (E_g) has been reduced exponentially from 2.11 eV to 1.55 eV. Electrical measurement illustrated that the resistivity also decrease exponentially with an increase in Ag content.

(Received June 9, 2015; Accepted August 10, 2015)

Keywords: Carbon thin films, Nano structures, Optical band gap, Electrical properties

1. Introduction

Graphite based multilayer films have attracted scientists and researchers [1,2] due to its dynamic applications with respect to optical, electrical, tribological and thermal properties [3,4]. This material has flexible optical properties due to its tunable optical band gap which can be achieved by changing sp^3 and sp^2 bonding ratio [4,5,6]. Graphitic films comprises of broad categories having properties ranging from graphite to graphene and up to crystalline diamond [7]. At present, metal containing graphite films were investigated to minimize its discrepancies about internal compressive stresses [12] due to variable amount of sp^3 bonding, so that it can be used in electronic and opto-electronic devices [8-10]. These composite films have been widely used for enhancement of dielectric constant and to develop multi channel devices [13]. Encapsulation of metallic nano particles in the structure of graphite has attracted much attention instead of using individual nano particles [14]. The physical properties of carbon's structure can significantly extend by incorporation of external atoms and species into these films by forming new microstructure [15]. These composite films reveal the properties of incorporated species as well as of the film matrix [16]. Literature survey depicts that metal incorporated DLC films can be synthesized either by doping metal tiny particles to form composite structured films [17,18] or by depositing multilayer of metal and carbon in a sequential manner on suitable substrates [19,34].

* Corresponding author: arslan.usman@ciitlahore.edu.pk

In the present work, thin multilayer films of Ag-graphite were deposited on Si (111) substrate via PLD in an on-axis geometry (vertically aligned). Structural, morphological, electrical and optical characteristics of the multilayered thin Ag doped graphite films were investigated in relationship with Ag content and compared with those reported in literature [20].

2. Experimental details

Multilayered thin films of graphite were deposited on a p-type Si (111) substrate via Pulsed Laser Deposition (PLD) system under ultrahigh vacuum achieved by turbo molecular pump. The PLD system as shown in Fig.1, consists of a vacuum chamber which was used to achieve vacuum of $\sim 10^{-6}$ torr. Before deposition a single crystalline Si (111) substrate was cleaned in 15% HF solution followed by ultrasonic cleaning to remove any oxide layer from the surface.

A KrF Excimer Laser 248 nm wavelength, 50 mJ pulse energy with a frequency of 20 Hz was used as a source of ablation from Ag-graphite target. The multi component target consists of a high purity graphite disc (diameter= 10 cm, thickness=1 cm) and a circular-shaped Ag strip (thickness=1 mm, diameter =1.5 cm) embedded in the centre of graphite disc. A UV lens (focal length= 20 cm) is used for focusing the laser beam on target's surface making an angle of 45° with its normal. The spot size of focused laser beam was approximately 0.45 mm², whereas the intensity and laser fluence were 2.3×10^8 W/cm² and 4.45 J/cm², respectively. The chamber contains an arrangement of target rotation (rpm=20) along with linear motion (step size = 1mm). Such arrangement helps in bringing different parts of target in front of laser beam for ablation; it also helps to avoid crater formation and to get uniform ablation of species from the target. The Si substrate was mounted on a substrate holder and was placed in front of target at $T_{\text{sub}}= 200^\circ\text{C}$ for all the depositions. Four Si(111) substrates were mounted on four sides of a squared shape substrate holder to get the same deposition environment for all films. The substrates were placed at a distance of 2 cm from target surface in vertically aligned positions.

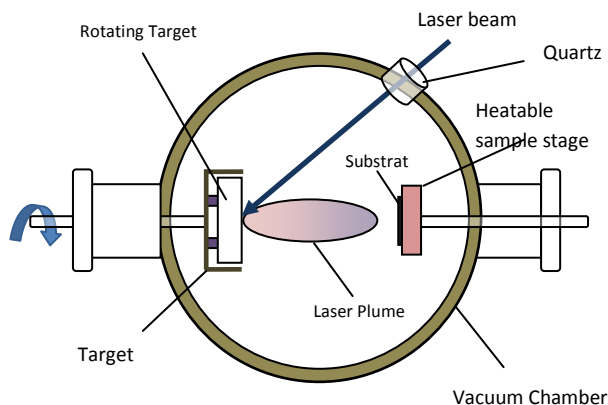


Fig.1. Schematic diagram of PLD system

Silver based multilayered thin films were prepared by taking laser shots on Ag and graphite part of multi-component target. These films were deposited such that four layers of Ag were sandwiched within five layers of graphite in each film. The concentration of graphite was kept constant (5000 laser shots) in all the films, whereas the concentration of Ag was the only variable parameter (400, 1200, 2000 and 2800 laser shots). This was attained by subsequent ablation from Ag and graphite parts alternatively from the multi-component target. So each graphite layer in the four Ag-graphite thin films contains 1000 laser shots on graphite part, whereas each Ag layer corresponds to 100, 300, 500 and 700 laser shots on Ag part in each layer, respectively.

3. Results & Discussion

3.1. X-ray diffraction analysis

X-ray diffraction patterns of multilayered Ag doped thin films are presented in Fig. 2, and the data obtained from it is listed in Table 1. The film consists of Ag planes grown in amorphous carbon film matrix. The Ag crystallites have been grown in this multilayered architecture. Fig. 2 represents the deposited films at varying Ag concentration. The diffraction peaks at 38.2° and 44.46° represents the silver (111) and (200) planes, respectively. It is evident from Fig. 2 that the preferentially oriented plane Ag (111) is dominant at all concentrations of Ag, whereas at higher concentration an additional plane Ag (200) grows substantially. The broad (111) diffraction peaks at the concentrations 400, 1200 and 2000 nm of Ag particles immersed in amorphous thin films, respectively. A sharp and high intensity peak of Ag (111) plane is observed in Ag-2800 thin film with a crystallite size of 65.4 nm. The crystallite sizes of Ag particles (Table 1) were calculated using the Scherer's formula [21];

$$D = k\lambda/\beta \cos\theta \quad (1)$$

where D is termed as crystallite size, k is a constant which is numerically equal to 0.95, $\lambda = 1.5406 \text{ \AA}$ is the wavelength of incident X-rays beam from $\text{CuK}\alpha$ source, β is FWHM of the peak and θ is the Bragg's angle. The dislocation line density $\delta = (1/D^2)$ and microstrain $\varepsilon = (\beta \cos\theta/4)$ for all the four samples were given in Table 1. Fig. 3 represents the crystallite size (D) of Ag particles and microstrain (ε) as a function of laser shots on Ag target. The graph shows that the crystallite size is increasing linearly for first three samples and increases rapidly at Ag-2800 (fourth sample). Whereas microstrain decreasing steadily with increasing concentration means that internal compressive stress decreases linearly with the increase in Ag concentration in the as grown multilayer thin film.

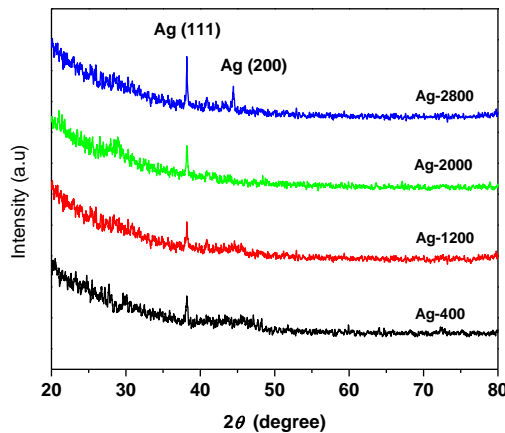


Fig. 2. XRD patterns of Ag-graphite multilayer thin films

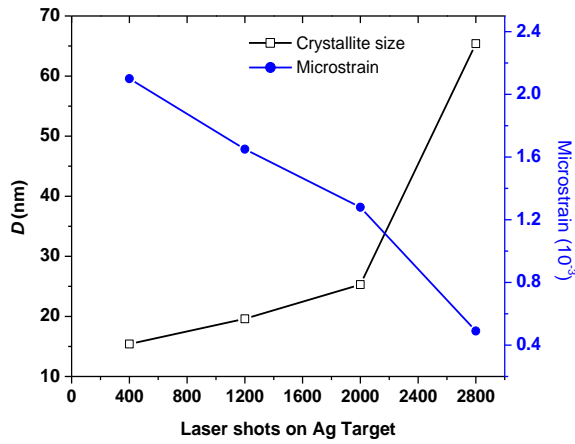


Fig. 3. Crystallite size and microstrain of Ag-graphite multilayer films as a function of laser shots on Ag target.

Table 1. XRD data of multilayer Ag-graphite thin films.

Sample	Peak	2θ (°)	d spacing (Å)	FWHM β (°)	Crystallite size D(nm)	Dislocation line density δ (10^{14} lines/m ²)	Microstrains (10^{-3})
Ag-400	Ag (111)	38.20	2.35	0.51	15.4	42.2	2.10
Ag-1200	Ag (111)	38.23	2.35	0.47	19.6	26.0	1.65
Ag-2000	Ag (111)	38.23	2.33	0.39	25.3	15.6	1.28
Ag-2800	Ag (111)	38.26	2.29	0.27	65.4	2.3	0.49
	Ag (200)	44.51	2.04	0.41	18.7	28.5	1.66

3.2. Raman Spectroscopy

Raman spectroscopy is used for the investigation and determination of ordering in carbon based films. The spectra shown in Fig. 4, describe two important characteristics of carbon films, the typical G band and its shoulder which is attributed as D bands at a lower wavenumber which becomes prominent at higher metallic concentration. G band is normally linked [22, 23] with the degree of graphitization. This effect is attributed to an increase in aromatic bonds and more specially for nano cluster formation of graphite its ordering and orientation [24, 25].

The Raman spectra describe the G band centre around 1560 cm^{-1} where as the D peak centre lies around from 1337 cm^{-1} . According to Robertson [26] the sp^2 sites possess variable bandgap, which depends on the arrangement of each sp^2 clusters, whereas the sp^3 sites acts as a tunnel barrier among sp^2 cluster. In an amorphous film matrix a cluster-cluster interaction was considered as main source of increased conductivity between sp^2 regions as a result of hopping process [23, 27]. In the same time an inhomogeneous disorder [26] was generated due to such distribution of sp^2 gaps. This disorder is the reason for broadening of the peaks at lower concentration. The Plasmon band reshapes its structure and a red-shifting is observed which in turn indicates the aggregation of nano clusters. A decrease in FWHM of G band is accredited to improved graphitization with the increasing metal composition which also reduced the inter layer

spacing. The peak below 1000 cm^{-1} corresponds to silicon due to lattice vibrations at some elevated deposition temperature.

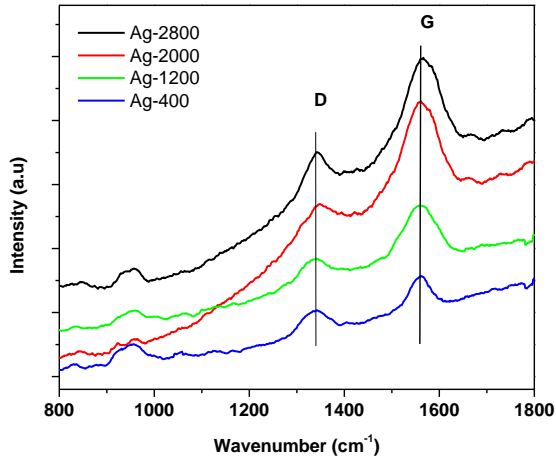


Fig. 4. Raman Spectra of the deposited Ag-graphite films

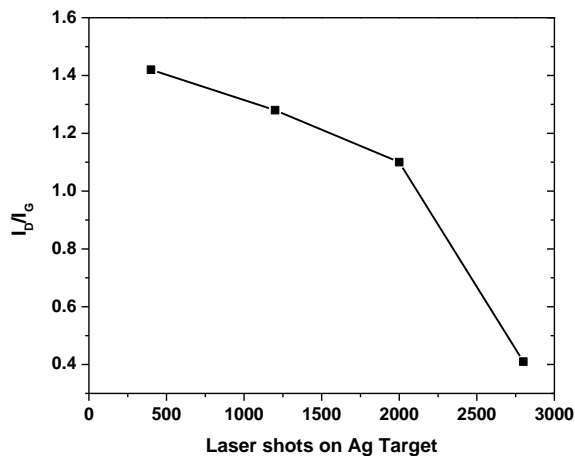


Fig. 5. I_D/I_G intensity ratio obtained for Raman spectra

The relative intensities ratio I_D/I_G is used to determine the phase and structural changes developed in the multilayer films. Fig. 5 describes the deviation in the I_D/I_G ratio with respect to Ag content, which reflects the presence of both sp^2 and sp^3 bonding in the films with an increasing proportion of sp^2 bonding as reported by Zeb et. al [28]. This variable proportion of sp^2 sites is a possible reason for enhanced clustering and increased chain length. As a result the graphitization is enhanced in the films. The sharp peak intensity with reduced FWHM for G band reflects the supremacy of sp^2 sites over sp^3 .

The kinetic process involved favors the formation of more stable sp^2 hybridization and as a result an aromatic layer is formed in the direction of incoming carbon species as discussed by Cappelli et. al. [29] which may be a possible reason for the formation of elevated inverted conical structures on the surface of multilayered films.

3.4. AFM Analysis

The AFM micrographs in Fig.7, describes the topography and development of texture at surfaces of multilayered thin films. Initially at lower concentration film consists of small clusters at surface due to aggregation of silver in the film's matrix. By gradually increasing the

concentration upto further aggregation and subsequently clustering takes place at surface which leads towards the nucleation of nanostructures. The formation of such carbon nanostructures can be attributed to a charge transfer process [35-37] due to accumulation of carbon atoms around Ag particulates. Surface roughness of the prepared films was analyzed using Nanotec WSxM 5.0 software [38]. The RMS roughness of the films are listed in table 2.

In Fig. 6, the data points are referring to RMS roughness of multilayered thin films as a function of Laser shots on Ag target. A straight line fitted to the data points by least-squares method gives the following relation (Eq. 2) with the linear correlation coefficient $r = 0.984$;

$$SR = 1.707 + 3.16 \times 10^{-3} LS \quad (2)$$

It describes that the surface roughness (SR) of the films increases by increasing Ag content, it varies from 2.41 nm to 10.1 nm.

Table 2: Roughness of the films deposited at varying Ag Concentration.

Sample	Elevated surface Structure (nm)	RMS roughness (nm)
Ag-400	12	2.41
Ag-1200	28	6.17
Ag-2000	40	8.34
Ag-2800	54	10.1

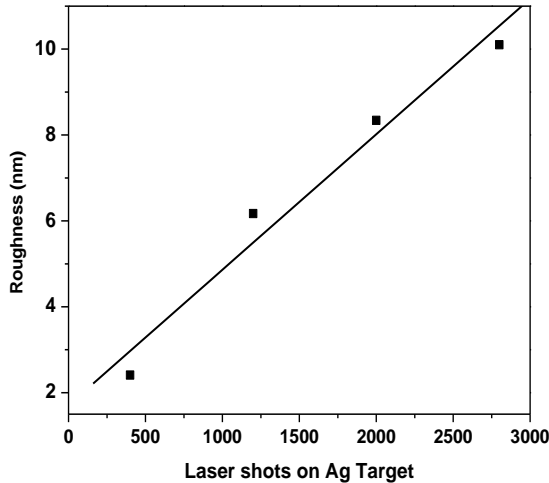


Fig. 6. Surface roughness of Ag-graphite multilayered films

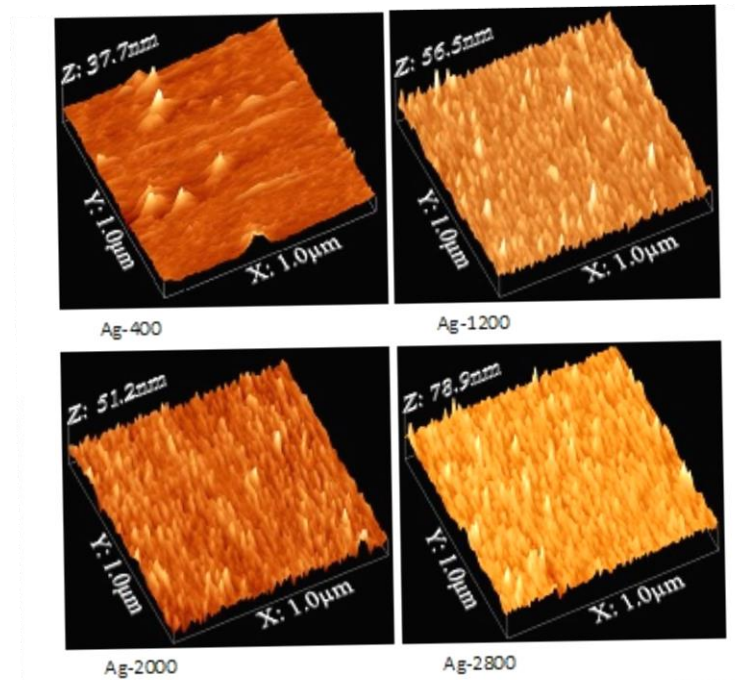


Fig. 7. 3D AFM micrographs of (a) Ag-400 (b) Ag-1200 (c) Ag-2000 (d) Ag-2800 multilayer thin films

3.3. Optical Characterization

Optical band gap (E_g) was determined [30, 31] by utilizing Spectroscopic ellipsometry technique using Cauchy model [32]. Optical band gap is calculated using absorption coefficient (α) and extinction coefficient (k), the absorption coefficient (α) may be expressed as;

$$\alpha = 4\pi k/\lambda \quad (3)$$

Where λ is incident beam's wavelength. The Tauc relation can be expressed through the relation [33]:

$$\alpha = (A/hv)\{hv - E_g\}^m \quad (4)$$

where A is material's constant, hv is photon energy, E_g is bandgap energy, the exponent m is theoretically bound to direct and indirect electronic transitions. Numerically its value for direct allowed transitions is equal to 1/2, and for forbidden transitions it is 3/2, similarly for indirect allowed and forbidden transitions it is 2 and 3, respectively. In this work, a plot of photon energy (hv) vs $(\alpha hv)^2$ was plotted for individual film. Optical bandgap (E_g) for direct transition with $m=1/2$ is calculated by extrapolation method applied to $(\alpha hv)^2 - hv$ curve. The x-intercept at $\alpha = 0$ gives the bandgap, therefore the estimated values of optical bandgaps were summarized in Fig. 8. Fig.8, links the dependence of band gap energy (E_g) of these multilayer films with number of laser pulses on Ag target. An exponential curve is obtained through the data points by applying least square fitting method which reveals that optical band gap of graphite thin film decreases exponentially from 2.11 to 1.55 eV as Ag concentration is increased.

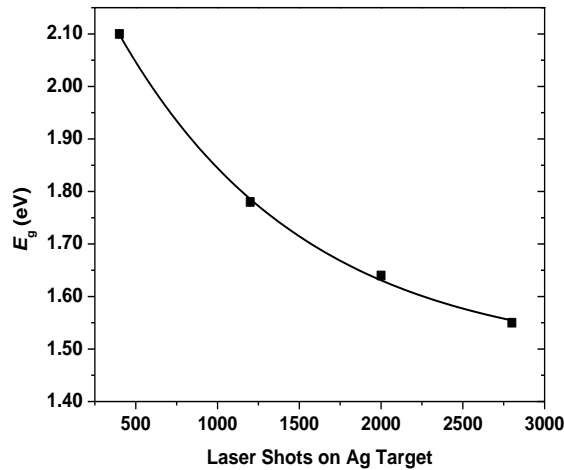


Fig. 8. Optical bandgap of multilayer Ag-graphite films deposited as a function on Laser shots on Ag target.

This trend is very much similar to the results reported by Ahmed et al. [31] for silver incorporated graphite films deposited on glass and silicon substrates via RF sputtering technique. They interrelated the decrease in E_g with the increase in sp^2 hybridization of DLC films as a function of increasing Ag content. Similarly, Sirajet. al. [34] have also reported that the Tauc plot in optical bandgap energy of multilayer DLC films deposited via PLD technique also decreases with increasing Co content. Siraj et al. [34] investigated via Raman spectroscopy that such trend is due to increase in sp^2 bonding and decrease in sp^3 bonding as a consequence of metallic concentration. This would mean that due to reduction of compressive stresses the dangling bonds that got passivated. This culminates as increased localized state which leads towards band tailing. This is an evidence for decreased bandgap energy as been observed

3.5. Electrical resistivity measurements

Electrical resistivity (ρ) measurements for graphite based Ag doped multilayer thin films was carried out by four point probe method. The formula [39] used for the calculation is described as:

$$\rho = F_c \times t \times R \quad (5)$$

where F_c is the correction factor ($= 2.96203$), which is a function of probe spacing and film dimensions, t is film's thickness, and R is resistance of the film. The value of R is based on the average of one hundred I-V measurements. On substituting the values in Eq. (5), the resistivity (ρ) values of Ag-graphite thin films were calculated. A Semi-log plot describes the relationship between resistivity and number of laser shots on Ag target for the deposited thin films as shown in Fig. 9.

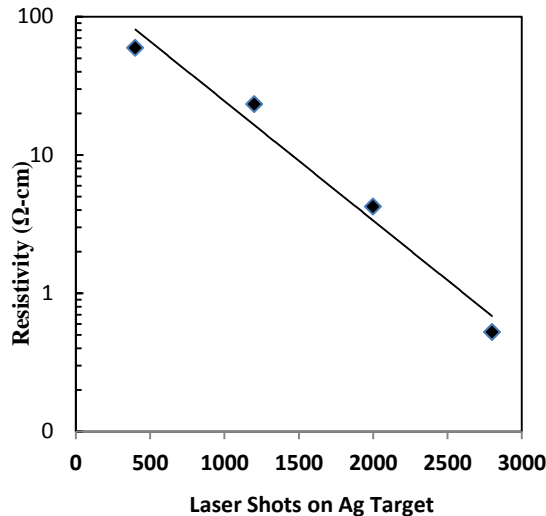


Fig. 9. Electrical resistivity of Ag-graphite multilayer thin films as a function of laser shots on Ag target in a semi-log plot.

It is revealed that with the increase of Ag content in deposited graphitic films the value of resistivity is decreasing. The least-square fit method when applied to the data points in Fig. 9 gives the relation:

$$\ln \rho = 5.18 - 2.0 \times 10^{-3} LS \quad (6)$$

Whereas the linear correlation coefficient $r = 0.9867$. It is observed that there is a sharp decrease in resistivity with increasing Ag content in multilayer films which is in good agreement with that reported for Ta-graphite and Ni-graphite films deposited at $T_{room} = 25^\circ\text{C}$ by PLD technique [40] along with that reported in the case of Ta-C:Mo composite films [41]. The decrease in resistivity of such kind of multilayer films can be linked to an increase in sp^2 cluster size and content rather than to the increase in metallic content only as reported by Pasaja et. al.[41]. As long as the conduction process in metal carbon multilayer thin films is concerned, it is not well fully understood. It is commonly believed that due to incorporation of metals into amorphous carbon film's architecture enhances the complexity of electronic transport properties, which is due to micron-size sp^2 clusters [42]. Along with electrical transport properties, tunneling and thermal activation coexist as reported by Huang et. al. [43] as a part of conduction process in Ag-graphite thin films; thermal process activates above 115 k where as tunneling dominates below this temperature.

4. Conclusion

The results pertaining to foregoing evidence on silver doped multilayer thin films deposited on Si substrate via PLD technique leads to the following conclusions.

1. Ag grows itself in the form of nano particulates without the formation of any carbide and an exponential increase crystallite size is observed from 15.4 to 65.4 nm.
2. The RMS roughness increases from 2.41 to 10.1 nm with the progressive rise in Ag concentration.
3. The optical band gap of the films reduced exponentially from 2.11 eV to 1.55 eV as an inverse relation to Ag content.
4. Electrical resistivity (ρ) of the multilayered films also decreased exponentially from 59.34 to 0.522 $\Omega\text{-cm}$.
5. I_D/I_G ratio also reduced with increasing content which is an indication of enhanced graphitization.

References

- [1] J.V.Rau, R.Teghil, A.DeBonis, A.Generosi, B.Paci, R.Generosi, M.Fosca, D.Ferro C, V.RossiAlbertini, N.S.Chilingarov, Diamond and Related Materials **19**, 7 (2010).
- [2] Jui Yun Jao, Sheng Han, Li Shen Chang, Ya-Chi Chen, Chi-Lung Chang, Han Chang Shih, Diamond and Related Materials **18**, 368 (2009).
- [3] N.W.Khun, E.Liu, Surface and Coating Technology **205**, 853 (2010).
- [4] K.M. Krishna, T. Soga, K. Mukhopadhyay, M. Sharon, M. Umeno, Solar Energy Materials and Solar Cells **48**, 25 (1997).
- [5] W. A. M. Kulisch, Deposition of Superhard Diamond-Like Materials, (Springer, Heidelberg, 1999), pp. 43-70.
- [6] G. Lazar, I. Lazar, J. Non-Crystalline Solids **331**, 70 (2010).
- [7] S. Adhikary, X.M. Tian, S. Adhikari, A.M.M. Omer, H. Uchida, M. Umeno, Diamond and Related Materials **14**, 1832 (2005).
- [8] J. Filik, P.W. May, S.R.J. Pearce, R.K.Wild, K.R. Hallam, Diamond and Related Materials **12**, 974 (2003).
- [9] Y. Lifshitz, Diamond and Related Materials **8**, 1659 (1999).
- [10] B. Bushan, Diamond and Related Materials **8**, 1985 (1999).
- [11] Q.Ou, T.Tanaka, M.Mesko, A.Ogino, M.Nagatsu, Diamond and Related Materials **17**, 664 (2008).
- [12] S. Kukielka, W. Gulbiński, Y. Pauleau, S.N. Dub, J.J. Grob, Reviews on Advanced Material Science **15**, 127 (2007).
- [13] A. Sylvestre, S. Kukielka, D.M. Nguyen, W. Gulbiński, Y. Pauleau, Reviews on Advanced Material Science **15**, 185 (2007).
- [14] M.Nagatsu, T.Yoshida, M.Mesko, A.Ogino, T.Matsuda, T.Tanaka, H.Tatsuoka, K.Murakami, Carbon **44**, 3336 (2006).
- [15] J. Robertson, Material Science Engineering R **37**, 129 (2002).
- [16] S.C.H.Kwok, G.J.Wan, J.P.Y.Ho, P.K.Chiu, M.Bilek, D.R.McKenzie, Surface & Coatings Technology **201**, 6643 (2007).
- [17] M. Andara, A. Agarwal, D. Scholvin, R.A. Gerhardt, A. Doraiswamy, C. Jin, R.J. Narayan, C.C. Shih, C.M. Shih, S.J. Lin, Y.Y. Su, Diamond & Related Materials **15**, 1941 (2006).
- [18] N. Menegazzo, C. Jin, R.J. Narayan, B. Mizaikoff, Langmuir **23**, 6812 (2007).
- [19] M.P. Delplancke-Ogletree, O.R. Monteiro, Surface & Coatings Technology **108–109**, 484 (1998).
- [20] NeerajDwivedi, Sushil Kumar, J. David Carey, R. K. Tripathi, Hitendra K. Malik,M. K. Dalai, ACS Applied Materials & Interface **5**, 2725 (2013).
- [21] R. John, S.S. Flrence, Chalcogenide Letters **7**, 269 (2010).
- [22] J.D. Carey, S.R.P. Silva, Phys. Rev. B **70**, 235417 (2004).
- [23] A. Ilie, A.C. Ferrari, T. Yagi, S.E. Rodil, J. Robertson, E. Barborini, P. Milani, J. Appl. Phys. **90**, 2024 (2001).
- [24] A.N. Obraztsov, O. Gröning, A.A. Zolotukhin, A.A. Zakhidov, A.P. Volkov, Diamond &Related Material **15**, 838 (2006).
- [25] C. Ducati, E. Barborini, P. Piseri, P. Milani, J. Robertson, J. Appl. Phys. **92**,5482 (2002).
- [26] F.R. Marciano, L.F. Bonetti, D.A. Lima-Oliveira, C.B. Mello, M. Ueda, E.J. Corat, V.J.Trava-Airoldi, Diamond & Related Materials **19**, 1139 (2010).
- [27] J.D. Carey, S.R.P. Silva, Phys. Rev. B **70**, 235417 (2004).
- [28] Shaista Zeb, MehboobSadiq, A. Qayyum, Ghulam Murtaza, M. Zakaullah, Materials Chemistry and Physics **103**, 235 (2007).
- [29] E. Cappelli, C. Scilletta, M. Servidori, V. Valentini, S. Orlando, Diamond & Related Materials **17**, 1476 (2008).
- [30] Toguchi M, Higa A, Shima T and Miazato M, Journal of Applied Physics **33**, 747 (1994).
- [31] Bhattacharyya D, Chaudhuri S, Pal A K and Bhattacharyya S. K, Vacuum **43**, 1201 (1992).
- [32] M. Sultan, R. Singh, Journal of Physics D: Applied Physics **42**, 115306 (2009).
- [33] J. Tauc, R. Grigorovici, A. Vancu, Physica Status Solidi A **15**, 627 (1966).

- [34] K. Siraj, M. Khaleeq-ur-Rahman, M.S. Rafique, M.Z. Munawar, S. Naseem, S. Riaz, Applied Surface Science **257**, 6445 (2011).
- [35] A. Usman, M.S. Rafique, M. Khaleeq-ur-Rahman, K. Siraj, SafiaAnjuma, H. Latif, Taj. M. Khan, M. Mehmood, Materials Chemistry and Physics **126**, 649 (2011).
- [36] A. Bozhko, T. Takagi, T. Takeno, M. Shupegan, Journal of Physics: Condensed Matter **16**, 8447 (2004).
- [37] K.I. Schiffmann, M. Fryda, G. Goerigk, R. Lauer, P. Hinze, A. Bulack, Thin Solid Films **347**, 60 (1999).
- [38] I.Horcas, R. Fernandez, J.M. Gomez-Rodriguez, J. Colchero, J. Gomez-Herrero, A.M. Baro, Review of Scientific Instruments **78**, 013705 (2007).
- [39] A.A. Ogwu, T.H. Darma, E. Bouquerel, Journal of Achievements in Materials and Manufacturing Engineering **24**, 172 (2007).
- [40] J.C. Orlianges, C. Champeaux, A. Catherinot, A. Pothier, P. Blondy, P. Abelar, B. Angleraud, Thin Solid Films **453–454**, 291 (2004).
- [41] N. Pasaja, S. Sansongsiri, S. Intarasiri, T. Vilaithong, A. Anders, Nuclear Instruments and Methods in Physics Research B **259**, 867 (2007).
- [42] S. Sansongsiri, A. Anders, B. Yotsombat, Diamond & Related Materials **17**, 2080 (2008).
- [43] Q.F. Huang, S.F. Yoon, Rusli, H. Yang, B. Gan, K. Chew, J. Ahn, Journal of Applied Physics **88**, 4191 (2000).